J. Synchrotron Rad. (2000). **7**, 374–381

Non-projectiveness of X-ray Pendellösung-fringed diffraction images

J. Yoshimura

Institute of Inorganic Synthesis, Faculty of Engineering, Yamanashi University, 4-3-11 Takeda, Kofu 400-8511, Japan. E-mail: yoshimur@ccn.yamanashi.ac.jp

(*Received 28 December 1999; accepted 7 August 2000*)

It has been experimentally found that X-ray moiré fringes are not exactly given as a projected figure from the specimen crystal as predicted by the standard theory of X-ray dynamical diffraction, but show a kind of spatial oscillation along the beam path out of the crystal. This paper reports that a similar spatial oscillation has been found for Pendellösung fringes in a similar experiment recording plane-wave X-ray topographs of a silicon wedge crystal onto a set of multi-stacked films. The oscillation of the Pendellösung fringes was easily found among the simultaneous topographs on the multi-stacked films by examining the fringe profiles, and was also found in topographic images by somewhat careful inspection. It is noteworthy that a simple reciprocal correspondence was observed between the amplitude of fringe oscillation and the fringe contrast. This finding of non-projectiveness, *i.e.* the fringe oscillation noted above, in Pendellösung fringes as well as in moiré fringes suggests that the non-projectiveness occurs as a very basic property of X-ray interference fringes produced by crystal diffraction.

Keywords: Pendellösung fringes; moiré fringes; interferometry; plane-wave topography; dynamical diffraction.

1. Introduction

It has been shown that moiré fringes observed in X-ray plane-wave topography are not exactly given as a projection of the intensity pattern on the exit surface of the crystal, but show a spatial oscillation in their positions and directions along the beam path out of the specimen crystal (Yoshimura, 1987, 1989, 1991, 1992, 1996*a*,*b*, 1997; Yoshimura & Ishikawa, 1990). This non-projectiveness (NPJ) disagrees with the prediction by the standard theory (*e.g.* Azaroff *et al.*, 1974; Authier, 1996) that X-ray diffraction interference fringes of any type should be a projected figure in the sense above, and thus has raised a basically significant question on moiré fringes. Experimental observations of such non-projective moiré fringes of various spacings and directions, made using bicrystal specimens and an X-ray interferometer (Yoshimura, 1991), and using conventional source and synchrotron radiation, indicate that NPJ is a general property of moiré fringes which appears manifestly in near plane-wave experiments. In a previous paper (Yoshimura, 1996*a*; see also Yoshimura, 1997), a full observation has been reported regarding the features of this fringe oscillation viewed in moiré topographs, intensity profiles, plots of the fringe position/direction, and a map of oscillation amplitude over a wide area. While the study of the NPJ in moiré fringes proceeds, we have recently found that similar NPJ also occurs in Pendellösung fringes, by inspecting topographic data of wedge crystals recorded in a preliminary experiment. The NPJ in Pendellösung fringes was clearly recognized by examining fringe profiles, though it was not so readily found in moiré fringes by casual observation of topographs. Also, in two-dimensional topographic images, small non-projective changes in the fringe pattern were found afterward by carefully searching in low fringe-contrasted areas in the topographs. This finding of NPJ in Pendellösung fringes will provide new prospects for the elucidation of NPJ. In this paper we report such an observation of Pendellösung-fringe NPJ.

2. Experimental procedure

2.1. *Recording of simultaneous Pendellösung topographs*

The experiment was conducted using synchrotron radiation at station BL-15C at KEK-PF, Japan, using the set-up illustrated in Fig. 1. The experimental procedure and conditions are almost the same as in the previous paper (Yoshimura, 1996*a*) except for a small change in the monochromator–collimator system. X-rays from the synchrotron source were monochromated and collimated by an Si 111 double-crystal premonochromator and an Si 220 asymmetric-reflection collimator of asymmetry factor $b = 1/40$. The wavelength of the incident X-rays onto the specimen was centred at $\lambda_0 = 0.72$ Å with a spread $\Delta\lambda/\lambda_0 \simeq 9 \times 10^{-4}$. The angular spread was $0.08''$ for individual wavelengths and $0.34''$ over the entire wavelength range. The specimen was a simple wedge crystal cut from a FZ silicon block, shown in Fig. 1(*b*). The exit surface was

cut to slope in two directions towards the entrance surface so as to give an oblique fringe system. The 220 reflection was used in the symmetric Laue geometry, the specimen being set in the parallel setting with the upstream Si 220 collimator. The incident intensity was known to be uniform within ±2.6% over the irradiated specimen by a densitometric analysis of the topographs.

In the imaging procedure, a plane-wave diffraction image of the wedge crystal with an accompanying Pendellösung fringe pattern (hereafter Pendellösung topograph) produced in the set-up above was recorded onto a set of 12 X-ray films simultaneously. The specimen was then set at the peak position of the rocking curve of the diffracted beam, though a theoretical study of the image intensity, undertaken after the experiment, shows that the specimen must have been slightly misaligned. Very thin (20 μm-diameter) Pt wires stretched in a rigid frame were placed between the specimen and the X-ray films so that the images of their shadows made a reference position and/or orientation on the topographs. The specimen-to-film distance, z_d, was 52.4–54.6 mm along the transmitted beam ($\mathbf{K}_0$). Recording X-ray films were placed parallel to each other with an almost constant interval, and the averaged film-to-film separation was 0.20 mm. The transmitted and diffracted beams (O and G beams, respectively) were incident on the X-ray films, making angles of 14.4° and 7.3°, respectively, to the normal to the film plane. This film orientation and z_d were determined after the experiment by measuring the distances between the O and G images of a point-like defect. The exposure time was 22 s. Single-coated X-ray films were specially prepared for this experiment from conventional-type high-resolution X-ray films (Fuji No. 50; undeveloped grain size 0.3 μm). The emulsion thickness was 10 μm. The intensity attenuation of X-rays due to film absorption was 6.7% per film. The set of simultaneous Pendellösung topographs which were chosen to be fully analyzed for this paper were recorded in this way. Besides this, several topograph sets were recorded with different film intervals and/or a different specimen, to serve as supplementary data for checking findings in the main data.

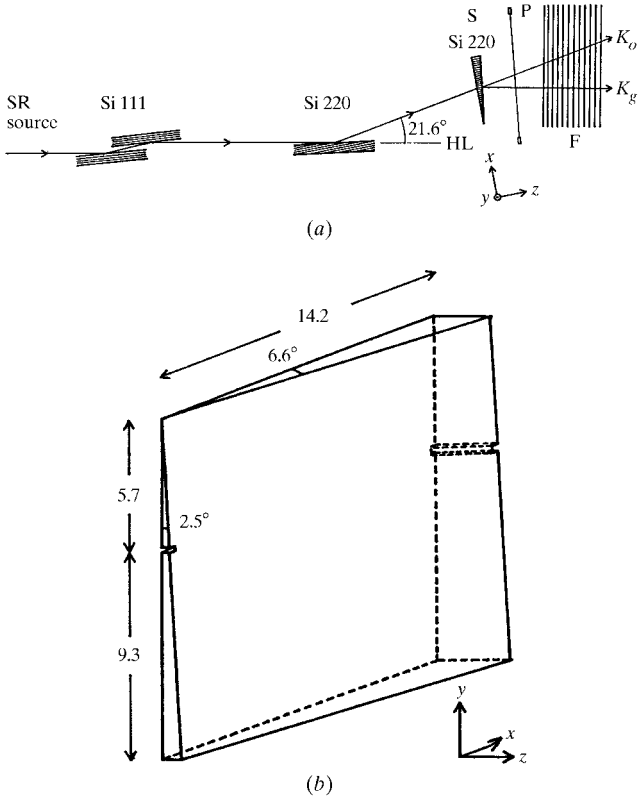

Figure 1
(*a*) Experimental set-up. S: specimen; P: thin Pt wire stretched in a rigid frame; F: X-ray films. x_e axis parallel to $[1\bar{1}0]$, y axis parallel to $[11\bar{2}]$, z_e axis parallel to [111]. The x_e and z_e axes lie in the vertical plane, and the chained line HL indicates the horizontal direction. (*b*) Detailed drawing of the specimen wedge crystal. Dimensions are given in mm.

2.2. *Image processing of Pendellösung topographs*

The photographic density, D, of some of the 12 topographs was measured using a microphotometer (Joyce–Loebl Mk 3CS) so that exact fringe profiles and fringe contrast were known. The effective slit area for illumination was 20 μm (width) × 50 μm (height). The main image analysis was conducted using an image processor (PIAS LA-525) with 256 grey levels. The image on the X-ray films was input into the processor with linear presetting, using an optical system equipped with a CCD camera. One pixel length in input images corresponds to about 20 μm on the real scale. These original input images received shading correction, contrast reversal, dynamic range expansion and smoothing. The smoothing was performed using a 3 × 3 matrix (a_{ij}) ($a_{ij} = 1$; $i, j = 1, 2, 3$) as space filter. Although the curve of grey level *versus* D was slightly non-linear in this processing, the non-linearity does not significantly matter in the analysis of fringe oscillation (see Yoshimura, 1996*a*).

2.3. *Theoretical calculation of image intensity*

The theoretical image intensity of Pendellösung topographs was calculated to have reference data with which the experimental image intensity and fringe profiles should be compared. A double-crystal arrangement with parallel setting for the Si 220 reflection and using σ-polarized Mo $K\alpha_1$ radiation was adopted in place of the actual experimental set-up. The image intensity was calculated using

$$I(x, y, \Delta\Theta) = \int R_1(\theta - \omega_0, b) R_2[\theta + \Delta\Theta + \omega(y), t(x, y)]\, \mathrm{d}\theta \Big/ \int R_1(\theta - \omega_0, b)\, \mathrm{d}\theta. \quad (1)$$

Here, $R_1(\theta)$ and $R_2(\theta)$ denote the intrinsic diffraction curves of the monochromator and the specimen crystal, respectively; (x, y) denotes the rectangular coordinates on the exit surface of the specimen; $\Delta\Theta$ denotes the rocking angle of the specimen, but was set at $\Delta\Theta = 0$ in this calculation; θ is the glancing angle of the incident beam; ω_0 is the angular deviation from the kinematical Bragg angle due to refraction; b is the asymmetry factor of diffraction

and was set at $b = 1/40$; $\omega(y)$ is the angular deviation due to the tilt of the specimen (misalignment), and was assumed to be $\omega(y) = 0.05 \times (y - 1.0)$ [see equation (48) of Yoshimura (1984)], where the value of 0.05 denotes the tilt angle divided by a constant proportional to the source-to-specimen distance in units of arcsec mm^{-1}, and $y = 1.0$ is the position at which the rotation axis of the tilt lies; $t(x, y)$ is the crystal thickness at a point (x, y).

3. Results

3.1. *Observation of Pendellösung topographs*

Fig. 2 shows one of the 12 simultaneous Pendellösung topographs. The *O*-beam image shown here, rather than the *G*-beam image, was chosen for the full analysis; there is no essential reason for this choice. Each topograph appears to be the same as that in Fig. 2 in rough unfocused observation, though very local inconspicuous changes can be seen among the topographs when inspected closely (Fig. 3). The method of treating these Pendellösung topographs is similar to that for treating the moiré topographs previously (Yoshimura, 1996*a*). The coordinates (X, Y) are taken on the image plane of the topographs, being by chance almost parallel to the (x, y) coordinates on the exit surface. The X-axis lies on the horizontal black line in the middle of Fig. 2. This and the crossing vertical lines are the shadows of the Pt lines placed between the specimen and recording films (the bending and the inclination of the vertical line are due to the so-bent and so-inclined Pt wire). The Y-axis is placed so as to pass on a point-like defect image beside the left horizontal cut. Quantitative analysis of the fringe oscillation (§3.3) was made within a rectangle of area 9.7 mm (X) × 8.0 mm (Y) shown in Fig. 2. Members of the simultaneous topograph set (T set) are numbered in increasing order of z_d, as $T1$, $T2$ *etc*. Pendellösung fringes are numbered from the left edge of the rectangle, as fringe 1, fringe 2 *etc*. The sense of the image contrast is taken such that white contrast indicates higher intensity, for reasons described in the previous paper (Yoshimura, 1996*a*).

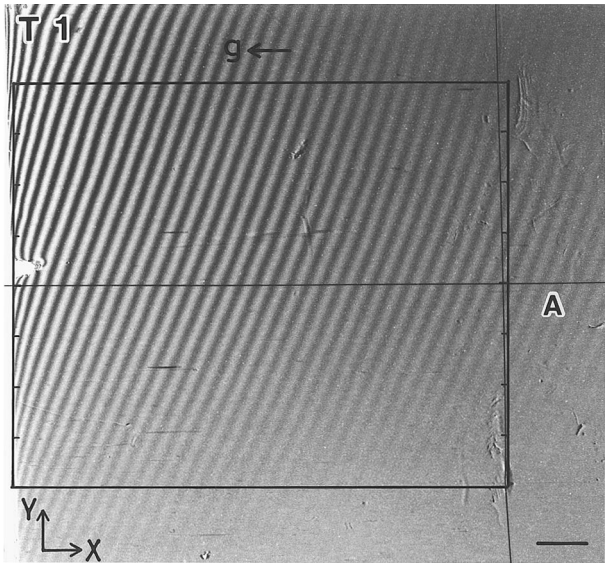

Figure 2
One of the simultaneous Pendellösung topographs studied in this paper. $T1$ topograph, T set No. 4, O-beam image. The scale bar represents 1 mm. **g** is the diffraction vector.

The specificity of the present Pendellösung topographs is as follows. The fringe spacing, though almost constant over the whole field, increases slightly from 0.27 to 0.32 mm over the first ten fringes (fringes 1–10), and then remains fixed at 0.33–0.35 mm. The fringe direction inclines by 30–33° from the Y-axis. Slight curvature of the fringe lines is due to the curved exit surface of the specimen. The fringe contrast, on the whole, decreases from upper left to lower right in the topographs and, in addition, shows a decrease from the middle towards the upper right-hand side of the field. The image intensity, or, more exactly, the peak intensity, of the fringes is at almost equal strength or increases slightly towards the $-Y$ direction, while decreasing towards the $+X$ direction. As far as is known by comparison with theoretical calculation, such variations in the fringe contrast and the image intensity are produced by the varying specimen thickness and slight deviation from the exact Bragg angle due to misalignment. The specimen is highly strain-free in the whole field, though the possibility of very slight residual strain in the upper right-hand corner cannot be completely excluded (in addition, short black lines and somewhat diffuse linear images showing some defects or flaws are not due to the specimen but arise from the monochromators upstream).

Fig. 3 compares the first four simultaneous topographs in a small area near the right-hand edge of Fig. 2 (marked A), to observe NPJ in the fringe pattern. A line of white contrast for the fringe peak just on the right of or above letters *a*, *b* and *c* may be seen to swing from side to side among the simultaneous topographs with a small amplitude. Further examples of such small local fringe oscillation can be seen in various places in Fig. 3. Among all the 12 topographs not shown here, we can see more clearly that such Pendellösung fringes repeat a spatial oscillation with an irregular amplitude and repetition cycle. A somewhat different form of the NPJ occurs in images of small strain centres, marked with vertical arrows. For example, the vertical arrow seen near the top edge shows such a clear change from white and black ($T1$), to largely black ($T2$), white and black again ($T3$), and largely black ($T4$). The insets show another example of such images showing an oscillatory change among the topographs. The change of the image contrast appears to be produced depending sensitively on the relative position of the strain centre to the main fringe system. Qualitatively, the image contrast of these strain centres is understood to be largely produced as the phase contrast of equal-inclination fringes, similarly to a previous observation by Ishikawa (1989). It seems natural to the present author to interpret the observations above as follows. The swinging fringes *a*, *b* and *c* and the image contrasts of the strain centres show that the phase of the

fringe system in the wave field oscillates along the beam path by some unknown effect. These oscillations in the Pendellösung fringes are quite similar to those observed in the moiré fringes previously, although a minor difference from the moiré fringes is that the large conspicuous oscillation of long fringe segments is difficult to find in the present Pendellösung fringes.

3.2. *Fringe profiles*

In Fig. 4 we show instances of fringe profiles measured using the microphotometer (Fig. 4*a*), along with the corresponding theoretical calculation (Fig. 4*b*). (The microphotometric trace in the $T2$ topograph is shown instead of the $T1$ trace for $Y = +1.9$ mm because the $T2$ trace allows a better comparison with a later image-processor trace by a better coincidence in the scanning y position; precise adjustment of the scanning position was difficult with the microphotometer used.) The measurement showed that the D value is 0.24–1.01 in this T set ($T1$–$T12$), with a fog density of about 0.14. The fringe contrast evaluated from the D value using the formula $V = (D_{max} - D_{min})/(D_{max} + D_{min})$, for example, ranges from 0.15 to 0.61 and from 0.06 to 0.28 in the two profiles in Fig. 4(*a*).

As seen from comparison between Figs. 4(*a*) and 4(*b*), theoretical calculation reproduces fairly well the maximum and minimum intensities of the experimental fringes. The assumption of the misalignment as described in §2.3 was necessary in order to obtain the overall good fitting

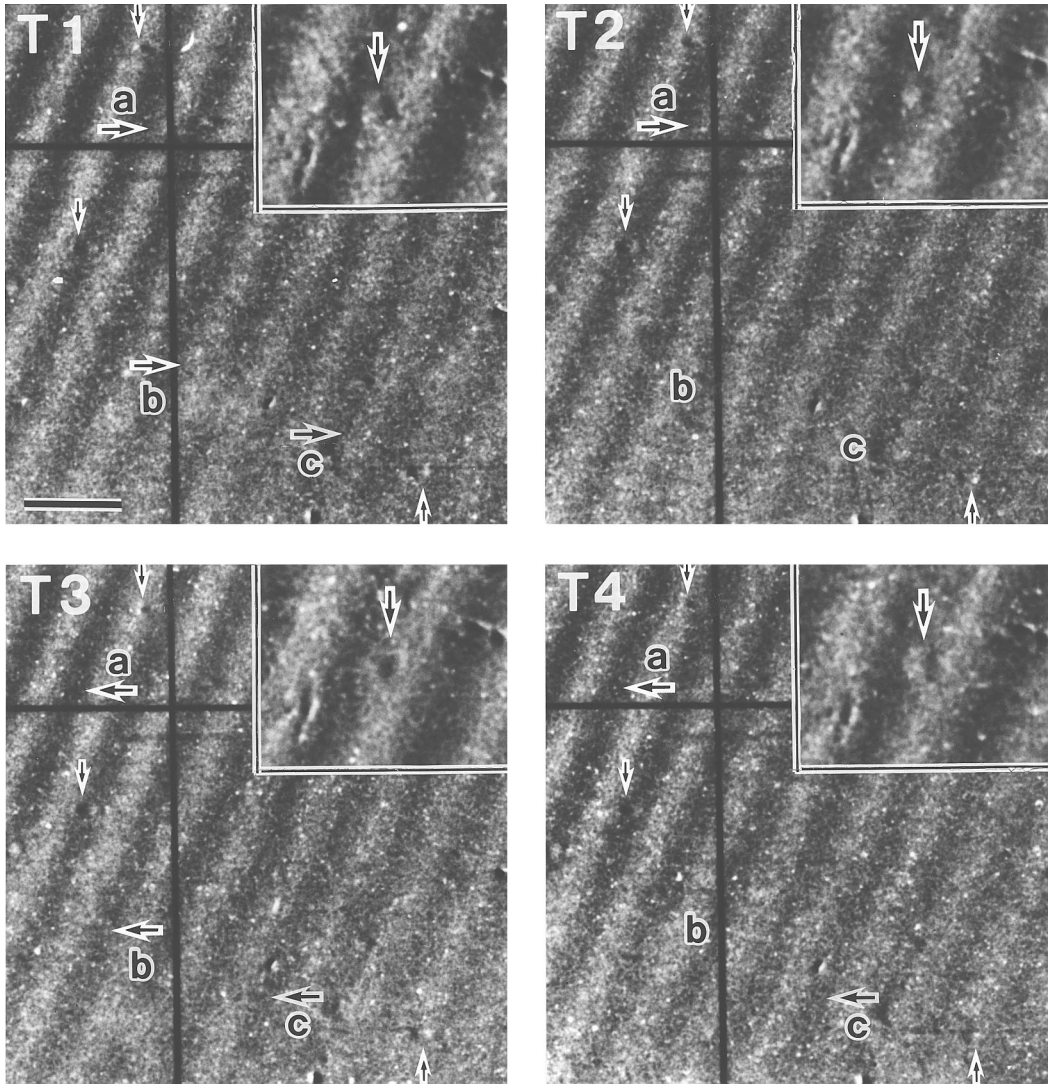

Figure 3
Comparison of Pendellösung-fringed diffraction images among members of the simultaneous topographs. A field near the right-hand edge in Fig. 2 (marked *A*) is observed at a higher magnification. Horizontal arrows *a*–*c* indicate the directions of displacement of the local segments of fringes just on the right of (*a*) or above (*b* and *c*) the arrows. Arrows are omitted in topographs where the relevant fringe segments are situated at an intermediate position in the whole side-to-side oscillation. Vertical arrows indicate images of small strain centres which show non-projective changes among the topographs. The insets also show another strain-centre image at a further higher magnification. The scale bar in topograph $T1$ represents 0.5 mm. The magnification of the insets is 1.67 times larger than that of the main topographs. The X and Y axes lie along the horizontal and vertical directions, respectively.

between theoretical and experimental curves in the entire field (Y = +4.0 mm to Y = −4.0 mm). It should be noted here that a great discrepancy between theory and experiment exists in the shape of the fringe profiles. The shape of the experimental fringe profiles gradually becomes asymmetric and irregular towards the $+X$ direction, whereas theoretical profiles keep on showing a highly accurate sinusoidal shape in the whole field. The progress of irregularity in the profile shape obviously seems to be in step with the decrease in the fringe contrast. Although no explanation is found here for the irregularity, it would be incorrect to ascribe the irregularity to the effect of strain, since the fringe pattern in Fig. 2 shows no disturbance by strain, and the intensity and fringe contrast in theory and experiment almost agree with each other.

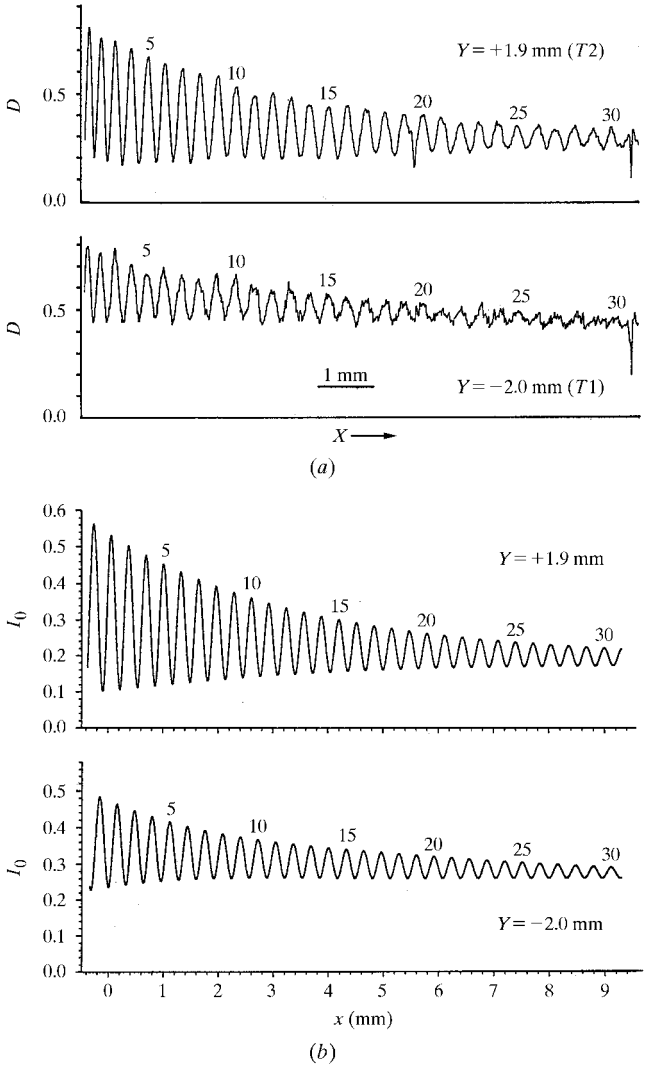

Figure 4
(*a*) Microphotometric traces of Pendellösung fringes, taken by scanning along the X axis on the $T1$ and $T2$ topographs. The ordinate is graduated in the D value after subtraction of the fog density. The numerals on top of the fringes denote the fringe numbers. (*b*) Theoretical calculation of the image intensity in Pendellösung topographs corresponding to the experimental profiles in (*a*). The ordinate is graduated in the diffraction intensity per unit intensity of the incident beam.

Fig. 5 compares profiles of Pendellösung fringes on member topographs of the T set in the output intensity from the image processor scanning along the X axis. The fringe-profile change occurring along the beam path of diffracted X-rays can be suitably investigated in this form of display. Profile scans at two Y positions are shown to give a good survey of the whole field of view. For easy comparison, the profile heights in all the member topographs, which decrease with the T number in the original films, are regulated to be roughly the same as each other by making a shading correction and a dynamic range expansion in the image processor (smoothing is not performed for profiles here). In spite of this processing, the relative profile height among several consecutive fringes in each topograph can be mutually compared reliably.

Remarks on the fringe profiles above are as follows:

(*a*) With regard to the occurrence and the amplifying of NPJ, the present Pendellösung fringes show a simple tendency dependent on the location in the field. As illustrated by the left-hand-side profiles in Fig. 5(*a*), fringes appearing with good contrast in the upper left quarter of the field have an almost symmetric-shaped profile, which shows almost no appreciable change among the successive member topographs. Pendellösung fringes in this partial field may be said to be an almost projected figure without apparent contradiction with conventional theory.

(*b*) Advancing towards the $+X$ direction, however, the asymmetric fringe profile gradually becomes more common and conspicuous in all member topographs. In addition, an appreciable change appears among the topographs in the direction and the degree of inclination of the asymmetric shape, and in the foot positions of the profile, so that an oscillation of the fringe-peak position results (fringes 22, 23, 29 *etc.* in Fig. 5*a*). An anomalous narrowing/broadening of the profile width and rise/fall of the peak height relative to neighbouring fringes may also be found (fringes 25, 30 *etc.* in Fig. 5*a*). A similar gradual rise in NPJ also proceeds with an advance towards the $-Y$ direction. As seen in Fig. 5(*b*), the profile shape generally becomes much more asymmetric and irregular so as to give a large fringe oscillation (fringes 18, 19, 26 *etc.* in Fig. 5*b*). The non-projective change of the profile width and relative peak height reaches a striking level (fringes 24–28), and double- and more multiple-peaked profiles appear containing finer ripples or spikes (fringes 17–30).

(*c*) As described above in detail, all five elementary changes of fringe profile mentioned for the previous moiré fringes (Yoshimura, 1996*a*) are found in the present Pendellösung fringes; they are changes in shape asymmetry, displacement of the foot position, profile width, relative peak height, and sub-peak structure of the profile. As illustrated by the mentioned fringes (No. 29 in Fig. 5*a etc.*), the shape-asymmetry change is generally accompanied by the displacement of foot positions in a manner similar to the moiré fringes (Yoshimura, 1996*b*); in other words, when

a fringe profile inclines to one side, the foot of the other side of the profile is displaced to the opposite direction to the inclination, so that the two changes contribute subtractively to the resulting peak shift. Furthermore, profile change proceeds in an almost continuous way among the topographs, accompanied by occasional discontinuous changes, and like-shaped profiles appear recurrently on low- and high-numbered topographs (fringes 19, 22, 23 *etc.* in Fig. 5*a*; 18, 23 *etc.* in Fig. 5*b*). In the relative peak-height change, pairs of neighbouring two fringes seem to repeat an in-phase oscillation over a few cycles [fringes (24, 25) and (26, 27) in Fig. 5*b*]. These features are commonly observed in much of the profile data, and hence do not seem to be an accidental result. They also indicate a similarity with the moiré fringes. From the observations above, it is clear that the NPJ of the present Pendellösung fringes is essentially the same as that of the previous moiré fringes.

(*d*) Additionally, it should be noted in this profile study that the five elementary changes of fringe profile tend to appear at different magnitudes of NPJ. As described in remark (*b*) above, shape-asymmetry change and displace-

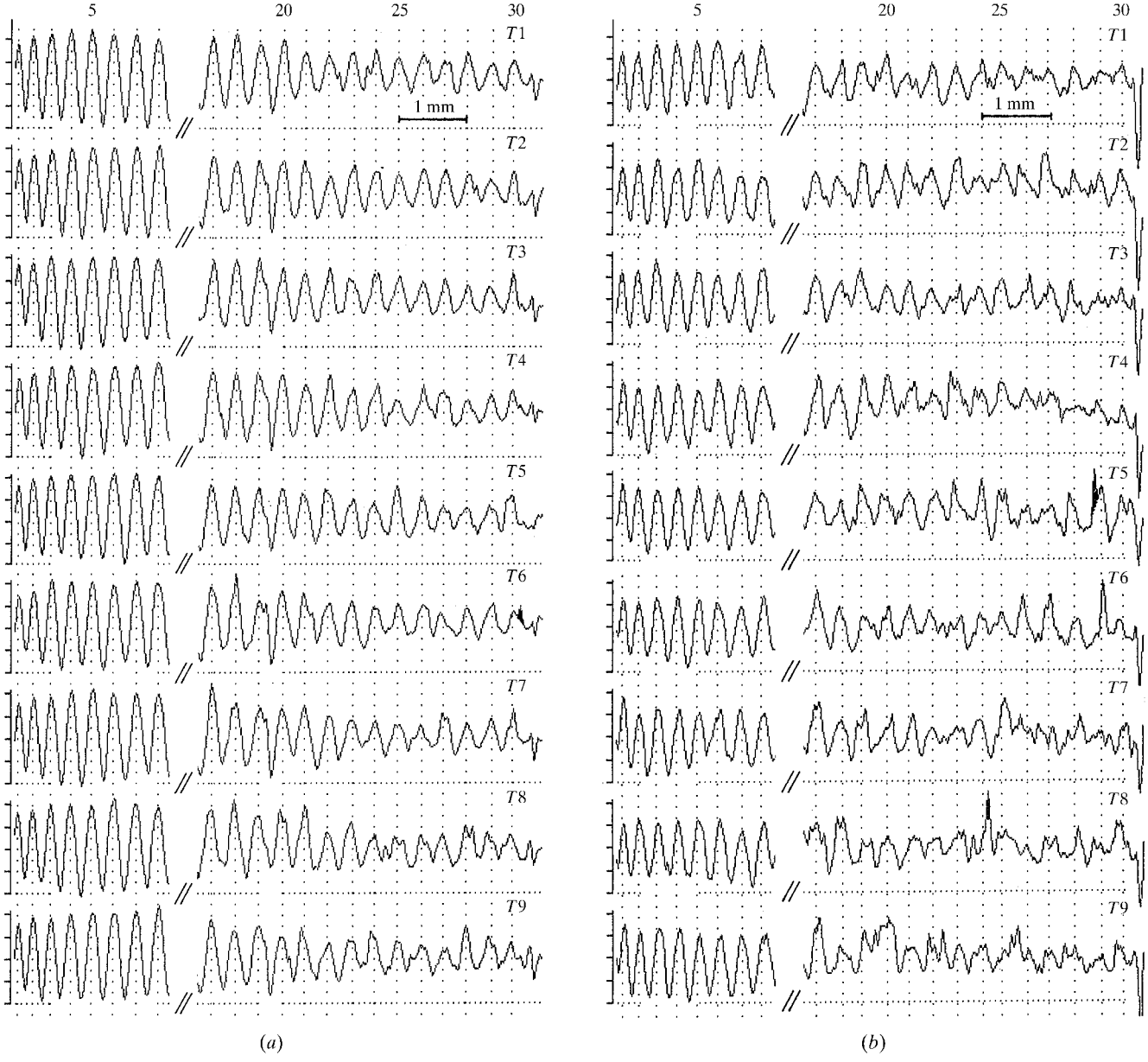

Figure 5
Intensity profiles of Pendellösung fringes compared among member topographs of the *T* set (the first nine of all 12 topographs). Output from the image processor scanning along the *X*-axis on the line (*a*) $Y = +1.9$ and (*b*) $Y = -2.0$. The numerals at the top denote fringe numbers. Vertical dotted lines are drawn for reference at the peak positions of fringes in *T*1. Deep drops on the right-hand edge are due to the shadow of the Pt line. Hatching [fringe 30, *T*6 in (*a*); fringe 29, *T*5, and fringe 24, *T*8 in (*b*)] shows an accidental noise in the recording films (small blurs or spots).

ment of foot positions first appear at a low level of NPJ, whereas the other three elements, such as relative peak-height change, begin to appear at a higher level.

(*e*) Finally, on the basis of the profile observation above, it seems obvious that the irregular profile shape (including asymmetric shape) and the non-projective profile change are produced by the same source. At least, if the irregularity of the profile shape does not occur at all, the non-projective profile change cannot occur either, since the latter is produced through the former as described in (*b*)–(*d*) above. Furthermore, it should be remarked that the non-projective profile change is always amplified where the fringe contrast decreases. Similar reciprocal correspondence has also been pointed out in moiré fringes (Yoshimura, 1996*a*). On the basis of a great many observations of profile data of NPJ so far, the mentioned correspondence does not seem an accidental coincidence, if not justified by theory for the moment.

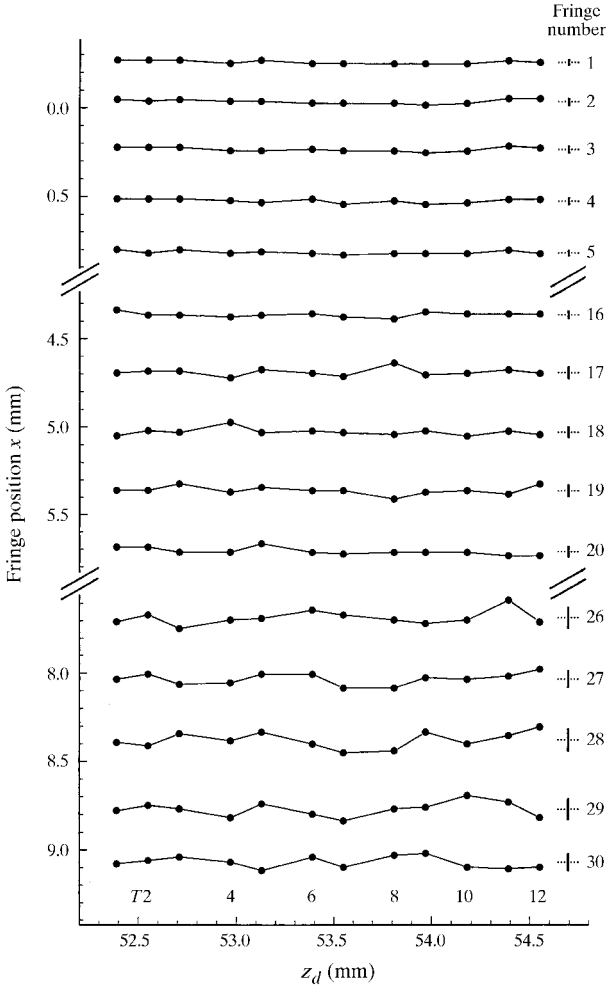

Figure 6
Plots of fringe position *versus* crystal-to-film distance z_d. Fringe positions determined on the line $Y = -2.0$ are shown. The numerals in the right-hand margin denote the fringe numbers, and the bars denote the oscillation ranges of the fringes (see text). The numerals below the plot of fringe 30 indicate the relevant member topographs.

3.3. *Fringe position plots*

As the first step of the quantitative analysis of complicatedly oscillating fringe profiles, we determine a fringe-position plot for the oscillating fringes. Similarly to the previous moiré fringes, the fringe position measured along the X axis was defined as the midpoint of the profile width at r times the peak height, r being 0.85. The peak height was measured from an assumed smooth background curve passing on the feet of fringe profiles. Profiles used in this procedure were of smoothed images of input topographs. Smoothing was still necessary for treating heavily disturbed profiles in the low-contrasted area, although profiles in most areas of the present Pendellösung topographs do not need smoothing. It should be mentioned that this quantification of the fringe oscillation is not sufficient in that information on the changes in profile width, peak height and sub-peak structure is not properly included. Fig. 6 shows an example of fringe-position plots, obtained for fringes shown in Fig. 5(*b*). The fringe oscillation can be viewed in a summarized form in such plots. The oscillation in the plots is somewhat milder than in the original profiles in Fig. 5(*b*), due to the use of smoothed profiles. Thick vertical bars on the right-hand edge indicate the oscillation range $\pm a_P$ of the respective fringes. Here, a_P denotes the oscillation amplitude determined by the formula $a_P = 2^{1/2}\sigma$, σ being the variance of the plot. This definition of amplitude is the same as in the previous moiré fringes. In spite of the mentioned omission of some profile-change elements, the amplitude thus defined can be a good measure for representing the magnitude of oscillation. The value of a_P is 0.7–0.9, 1.0–1.6 and 2.3–3.1 in pixels for the upper, middle and lower groups of fringes in Fig. 6, respectively. These values correspond to 5–6%, 6–9% and 13–17%, respectively, of the fringe spacing. Oscillations included in the beam path length (2.2 mm) from $T1$ to $T12$ appear to be roughly two cycles in fringes with large amplitude like the lower group in Fig. 6, though the oscillation frequency is not clearly countable because of the irregular oscillation.

4. Concluding remarks

Essentially the same NPJ as in the previous moiré fringes has been found in Pendellösung fringes emerging from a simple wedge crystal. Non-projective changes in Pendellösung topographs and in the intensity profiles of fringes have been observed to occur with detailed features similar to the moiré fringes. The finding of the NPJ in simple Pendellösung fringes as well as in moiré fringes suggests that this NPJ occurs as a very basic property of X-ray interference fringes produced by crystal diffraction. In the observation of NPJ above, special attention has been paid to apparent reciprocal correspondence between the magnitude of NPJ and the fringe contrast. Quantitative experimental data analysis on this point will be reported elsewhere.

The experiment was conducted under the approval of the Photon Factory Program Advisory Committee (proposal No. 90–113). The author gratefully acknowledges Dr T. Ishikawa for the preparation of the experimental set-up at the Photon Factory. The author thanks Dr K. Ito for the convenience of using the microphotometer at the Photon Factory.

References

Authier, A. (1996). *International Tables for Crystallography*, Vol. B, edited by U. Shmueli, §5.1. Dordrecht: Kluwer Academic Publishers.

Azaroff, L. V., Kaplow, R., Kato, N., Weiss, R. J., Wilson, A. J. C. & Young, R. A. (1974). *X-ray Diffraction*, pp. 176–438. New York: McGraw-Hill.

Ishikawa, T. (1989). *Rev. Sci. Instrum.* **60**, 2490–2493.

Yoshimura, J. (1984). *J. Appl. Cryst.* **17**, 426–434.

Yoshimura, J. (1987). *Acta Cryst.* A**43**, C221.

Yoshimura, J. (1989). *J. Phys. Soc. Jpn*, **58**, 1283–1295.

Yoshimura, J. (1991). *Acta Cryst.* A**47**, 139–142.

Yoshimura, J. (1992). *J. Crystallogr. Soc. Jpn*, **34**, 19–26. (In Japanese.)

Yoshimura, J. (1996*a*). *Acta Cryst.* A**52**, 312–325.

Yoshimura, J. (1996*b*). *Acta Cryst.* A**52**, C496.

Yoshimura, J. (1997). *Acta Cryst.* A**53**, 813.

Yoshimura, J. & Ishikawa, T. (1990). *Acta Cryst.* A**46**, C424–425.